Suppression of cofilin-1 promotes invasion in 3D hyaluronic acid matrices by promoting actin-based protrusions

Vivien D. Tran[®], and Sanjay Kumar^{a,b,c,d,*}, Lu Ling^b, Miles Duong^c, and Sanjay Kumar^{a,b,c,d,*}

^aUC Berkeley-UCSF Graduate Program in Bioengineering, San Francisco CA 94143; ^bDepartment of Bioengineering, University of California, Berkeley, CA 94720; ^cDepartment of Chemical and Biomolecular Engineering, University of California, Berkeley, CA 94720; ^dDepartment of Bioengineering and Therapeutic Sciences, University of California, San Francisco, San Francisco, CA 94158

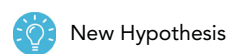
ABSTRACT Contributions of the actin turnover machinery to cell motility have been extensively studied in traditional two-dimensional (2D) culture paradigms. However, much remains unknown about how these proteins contribute to three-dimensional (3D) motility, particularly in matrices lacking strong contact guidance cues. Here, we explore this question in the context of glioblastoma (GBM) cell invasion through 3D hyaluronic acid (HA) hydrogels. We begin with a CRISPR screen to identify contributions of core actin turnover proteins to migration speed in 2D and 3D. Although suppression of most proteins reduced motility in both 2D and 3D, suppression of cofilin-1 (CFL) increased migration speed in 3D. CFL knockout cells uniquely formed longer and more protrusions in 3D compared with non-targeting control cells. Consistent with the screen, targeted CFL short hairpin RNAmediated knockdown (KD) decreased motility on 2D HA but increased motility in 3D HA. This effect appears HA-specific, as CFL KD did not increase motility in 3D collagen or in a transwell assay. Myosin X, CD44, and hyaluronidase-2 all localized to a subset of protrusions irrespective of cellular CFL status, implying that CFL suppression promotes filopodia and microtentacle extension. We propose that loss of CFL promotes the actin filaments in these protrusions, enabling GBM cells to penetrate 3D HA matrices.

SIGNIFICANCE STATEMENT

- Actin turnover is an important driving force behind cell motility. How the proteins in the actin
 turnover machinery contribute to cell motility in 3D matrices remains incompletely understood.
- The authors compared 2D and 3D GBM cell motility using HA hydrogels and identified through a CRISPR screen that CFL suppression increases motility speed through 3D HA matrices but not on 2D HA surfaces. They further find that loss of CFL increased the number and length of cellular protrusions.
- These findings suggest that CFL suppression promotes actin filaments within protrusions, enabling faster motility in 3D HA matrices.

Monitoring Editor Alexander R. Dunn Stanford University

Received: Sep 5, 2024 Revised: Jun 2, 2025 Accepted: Jun 30, 2025



INTRODUCTION

Cell migration is critical to many biological processes, including wound healing, embryogenesis, and cancer progression. To navigate through three-dimensional (3D) extracellular matrix (ECM), cells must dynamically remodel their cytoskeleton to adapt to ECM characteristics, including mechanics, micro/nanostructure, and degradability (Yamada and Sixt, 2019). This complex process requires coordinated action of many molecular components, with the actin cytoskeleton playing a central role in cell locomotion (Wyckoff et al., 2006; Yamaguchi and Condeelis, 2007). A core group of actin-binding proteins is responsible for driving actin disassembly and turnover within the cell (Goode et al., 2023). These factors—including cofilin (CFL), profilin (PFL), twinfilin (TWF), gelsolin (GSN), Srv2/cyclase-associated protein (CAP), and actininteracting protein 1/WD repeat protein 1 (WDR)—stabilize or modulate the actin network as needed to facilitate navigation through the ECM (Balcer et al., 2003; Pollard and Borisy, 2003; Goode et al., 2023).

CFL has been particularly extensively studied and shown to play crucial roles in directing two-dimensional (2D) migration. CFL activity status has also been noted as a phenotypic marker of cancer cell invasiveness (Wang et al., 2006; 2007; Bravo-Cordero et al., 2013). We have shown previously that CFL-1 (hereafter simply referred to as CFL), an actin severing protein phospho-inactivated by LIM kinase (LIMK), a downstream effector of the Rho GTPases, is required for front-back polarization of stress fiber networks and formation of organized lamellipodia in 2D motility over rigid surfaces (Lee and Kumar, 2020). Our work was motivated in part by studies from Lappalainen and colleagues, who showed that CFL may "prune" low-tension actin bundles from the leading edge, thereby deselecting these bundles from incorporation into highly contractile stress fibers (Tojkander et al., 2015). In our study, U2OS cells with suppressed CFL expression accumulated low-tension actomyosin bundles (as measured by femtosecond laser ablation) and failed to establish a unified leading edge, implicating CFL in establishing the front-back polarity needed for directional 2D migration (Lee and Kumar, 2020). In separate work, we demonstrated that suppression of LIMK 1 and 2 in glioblastoma (GBM) cells disrupted actin organization and lamellipodia protrusion and dynamics on 2D surfaces, which ultimately also disrupted cell polarization. LIMK1/2 knockdown (KD) cell-based tumors were also less invasive in vivo and produced longer survival times compared with control tumors. This observation was attributed to an overabundance of unphos-

This article was published online ahead of print in MBoC in Press (http://www.molbiolcell.org/cgi/doi/10.1091/mbc.E24-08-0384) on July 9, 2025.

Author contributions: V.D.T. and S.K. conceived and designed the experiments; V.D.T., L.L., and M.D. performed the experiments; V.D.T. and K.Y.A. analyzed the data; V.D.T., S.K., and K.Y.A. drafted the article; V.D.T. prepared the digital images; S.K. supervision and project administration.

Conflicts of interest: The authors declare no financial conflict of interest.

*Address correspondence to: Sanjay Kumar (skumar@berkeley.edu).

Abbreviations used: ADF, actin depolymerizing factor; CAP, Srv2/cyclase-associated protein 1; CFL, cofilin-1; ECM, extracellular matrix; GBM, glioblastoma; GSN, gelsolin; HA, hyaluronic acid; HA-only, HA matrix without RGD motifs; HA-RGD, HA matrix with RGD motifs; KD, knockdown; KO, knockout; LIMK, LIM kinase; McTNs, microtentacles; MyoX, myosin 10; NC, noncoding; NT, nontargeting; PFN, profilin-1; RGD, Arg-Gly-Asp; shRNA, short hairpin RNA; TWF, twinfilin-1; WDR, actin-interacting protein 1/WD repeat protein 1.

© 2025 Tran et al. This article is distributed by The American Society for Cell Biology under license from the author(s). Twelve months after publication it is available to the public under an Attribution–Noncommercial–Share Alike 4.0 Unported Creative Commons License (http://creativecommons.org/licenses/by-nc-sa/4.0).

"ASCB®," "The American Society for Cell Biology®," and "Molecular Biology of the Cell®" are registered trademarks of The American Society for Cell Biology.

phorylated CFL and thus increased CFL activity and a deficiency of actin filaments with the cell body (Chen et al., 2020). Taken together, the results support the notion that tight regulation of actin turnover is critical for effective 2D migration. However, it is unclear how these mechanisms and more broadly the systems that control cell front-back polarity in 2D govern motility in environments that are not permissive of formation of lamellipodia, that is, in confined substrates or in 3D ECM (Caswell and Zech, 2018; Yamada and Sixt, 2019). As described below, the picture is particularly unclear in 3D matrices that lack fibers or other directional contact guidance cues.

Cell migration has been historically studied on 2D tissue culture surfaces, a powerful and simple paradigm that is amenable to high-resolution imaging and mechanical characerization. However, cells navigating though tissues are often surrounded by a 3D ECM, sometimes encountering topographical cues absent in flat 2D substrates, including steric confinement, fibers, or bundles that may serve as contact guidance cues, and adhesions in all directions (Baker and Chen, 2012). Cells also display more migration modes in 3D, while in 2D cells often but not exclusively utilize flat, fan-shaped F-actin-based protrusions termed lamellipodia (Ridley et al., 2003; Petrie and Yamada, 2012). Much of what is known about the role of the actin turnover machinery in 3D migration comes from fibrillar matrices, including collagen and fibrin. In these matrix environments, the mechanisms of cellular migration, particularly of actin organization and turnover, are highly dependent on dimensionality and the biophysical properties of the matrix (Sanz-Moreno and Marshall, 2010; Doyle et al., 2013; Yamada and Sixt, 2019). The morphological linearity imposed by adhesion to fibers often induces alignment of focal adhesions and the actin cytoskeleton, which depends on the tight regulation of actin polymerization dynamics (Balzer et al., 2012; Carey et al., 2015; Guetta-Terrier et al., 2015; Monzo et al., 2016). For example, in one study with fibrillar cell-derived matrices and Matrigel, inhibition of LIMK did not affect the 2D motility of breast cancer cells. Conversely, the attenuated LIMK activity slowed 3D invasion by impairing invadopodial maturation and matrix degradation (Scott et al., 2010). Invadopodia have also been robustly induced by high density fibrillar collagen, whereas cell-derived fibronectin, gelatin, and low density collagen induce invadopodia to a much lesser extent (Artym et al., 2015). In a similar vein, in collagen matrices, fibroblast motility is associated with the development of either 2D-like lamellipodia or lobopodia, which are driven by hydrostatic pressure rather actin polymerization-driven protrusions. The type of protrusion depends on the degree to which the matrix exhibits nonlinear elasticity (Friedl et al., 2012; Petrie and Yamada, 2012). Collectively, these examples demonstrate the need to examine cell migration in a physiological context, as both actin organization and the associated intracellular signaling vary widely between each mode of

Although the studies discussed above have lent tremendous insight into mechanisms of 3D migration, comparatively little is known about the mechanisms of cell migration through defined, nonfibrillar, tissue-mimetic matrices, such as hyaluronic acid (HA). HA is major component of the brain parenchymal ECM, which is much less abundant in collagen, fibronectin, and laminin compared to most conenctive tissues and thus lacks many of the associated fibrillar contact guidance cues (Bellail et al., 2004). We have previously characterized a mode of migration utilized by GBM cells to navigate through 3D HA-rich matrices that involves long, thin actin/microtubule-based protrusions termed microtentacles (McTNs). McTNs adhere to HA via CD44 and are laden and stabilized by both actin and microtubules, both of which distinguish

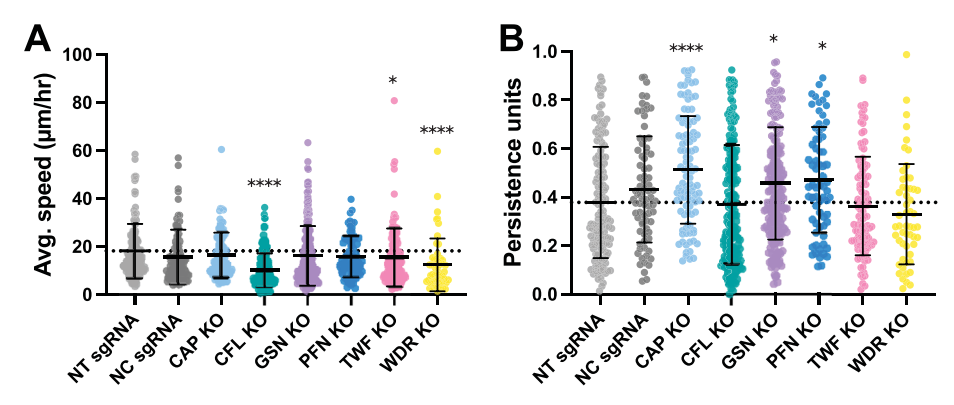


FIGURE 1: Random single-cell motility of CRISPR KO cells on 2D HA-RGD gels. Cells were tracked for 46 points over a period of 7.75 h, with 10 min between each point. (A) When compared with NT control cells, CFL KO, TWF KO, and WDR KO cells have significantly slower average speeds. (B) CAP KO, GSN KO, and PFN KO have significantly higher persistence compared with NT control. For both graphs, the dashed lines denotes the mean value of NT sgRNA control and error bars represent mean with SD. *P < 0.05; ****P < 0.0001 by Kruskal–Wallis test followed by Dunn's multiple comparisons test.

these structures from filopodia or lamellipodia (Wolf et al., 2020). Our and others' findings therefore suggest noncanonical roles for the actin turnover machinery in nonfibrillar 3D matrices, inviting deeper investigation (Poincloux et al., 2011; Balzer et al., 2012; Shibue et al., 2013; Djuzenova et al., 2015; Carmona et al., 2016).

In this study, we explore contributions of the actin turnover machinery to 3D motility in the context of GBM invasion through HA matrices. By applying a targeted CRISPR knockout (KO) screen to a panel of core actin turnover proteins, we find that CFL suppression results in faster 3D invasion, whereas suppression of other targets slows invasion. Protrusions formed by CFL KO cells are longer and more abundant than those of control cells, suggesting that CFL suppression increases invasion in 3D HA through actin polymerization. Studies with short hairpin RNA (shRNA)-mediated CFL suppression independently corroborate this observation and further reveal the effect to be HA-specific, with no increase in motility in 3D collagen or transwell paradigms. Molecular characterization reveals both filopodial and McTN markers in subsets of protrusions. Our results collectively support a mechanism in which CFL suppression promotes protrusion function through F-actin polymerization, thereby enhancing penetration through 3D HA matrices and facilitating invasion.

RESULTS

CFL is unique among actin-disassembly factors in driving 3D migration through HA matrices

To begin examining how the systems that govern actin turnover machinery on 2D substrates translate to 3D contexts, we conducted a limited CRISPR-Cas9 KO screen to systematically assess contributions of actin-binding proteins to 2D and 3D motility. Based on our previous work that supported a model in which cell front-back polarity is driven in part by CFL activity and actin turnover, we focused on targets that are part of the core actin disassembly-promoting machinery. These factors mediate actin turnover to reorganize the actin cytoskeleton as the cell navigates the ECM (Balcer et al., 2003; Pollard and Borisy, 2003; Goode et al., 2023). For proteins with more than one isoform, we chose to knock out the most abundantly expressed isoform in human cells; the abbreviations for each protein hereafter denote that isoform. Our resulting targets were CFL (specifically CFL-1), PFN (specifically PFL-1), TWF (specifically TWF-1), GSN, Srv2/CAP, and WDR.

To create the KO cell lines, we sequentially delivered via lentivirus Cas9 cDNA and sgRNAs targeting the gene of interest, generating cell lines that stably expressed Cas9 along with sgRNAs and producing a mixture of indels. Control cell lines were created by using sgRNAs that targeted non-coding (NC) regions of the genome or were non-targeting (NT).

To compare 2D and 3D motility within a nonfibrillar matrix, we cultured U251 GBM cells (Pathak and Kumar, 2012; Bangasser et al., 2017) in or on engineered HA hydrogels, which mimic brain ECM and have been used in our previous work to dissect molecular mechanisms of GBM invasion (Ananthanarayanan et al., 2011; Kim and Kumar, 2014; Chen et al., 2020; Wolf et al., 2020; Amofa et al., 2024; Cha et al., 2024; Garcia et al., 2024). HA hydrogels may be fabricated with brain-like elastic moduli (10 Pa – 1 kPa) and functionalized with RGD-based peptides to allow integrin engagement (Ananthanarayanan et al., 2011; Wolf et al., 2020). The HA matrix is cross-linked with matrix metalloprotease-degradable peptide sequences, and the matrix backbone itself may be degraded via cell-derived hyaluronidases (Ananthanarayanan et al., 2011).

We first examined 2D random, single-cell motility of our KO cell lines on HA conjugated with RGD (HA-RGD) to establish baseline migratory phenotypes. Cells were allowed to spread and adhere on the gels for 4 h before timelapse imaging. CFL, TWF, and WDR KO cells displayed significantly reduced cell speed during a timelapse of 7.5 h compared with NT control, indicating that loss of these actin-binding proteins hampered the cells' ability to migrate in 2D (Figure 1A). These results match previous studies of the role of these proteins (CFL, TWF, and WDR) in 2D migration, consistent with their established role in lamellipodial extension (Goode et al., 2023). CAP, GSN, and PFN KO cells had increased persistence relative to controls (Figure 1B).

To examine the effects of depletion of these proteins on 3D motility, we conducted 3D spheroid invasion assays in HA-RGD gels cross-linked with protease-degradable linkers. We hypothesized that CFL, TWF, and WDR KO would diminish 3D motility based on the results of the 2D motility assay. After 4 d of invasion in HA-RGD gels, CFL KO cells surprisingly displayed the highest migration speed of all cell lines, including controls, as measured by area change (Figure 2B) and maximum cell distance from the core spheroid (Figure 2C). This result was the opposite of 2D, where CFL KO led to slower cell migration (Figure 1A). The other KO lines did



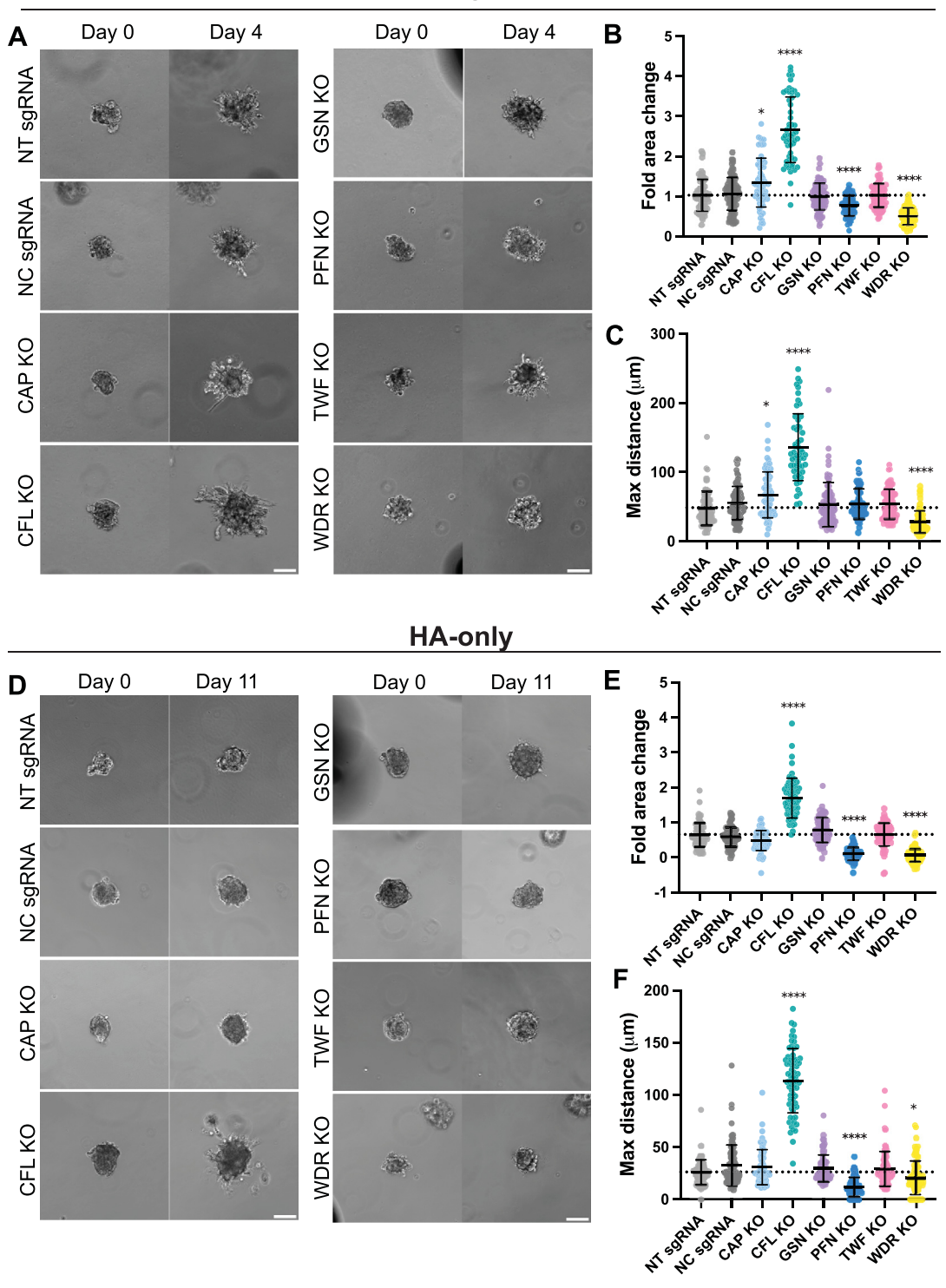


FIGURE 2: 3D spheroid invasion assay of CRISPR KO cells in 3D HA gels. (A) Representative brightfield images of spheroids at day 0 and 4 for each cell line in HA-RGD gels. (B) Calculated fold area change of day 4 normalized to day 0 area of spheroids. CFL KO shows significant increase compared with NT control, while PFN KO and WDR KO significantly decrease area change. (C) Maximum cell distance from the sphere edge. CFL KO shows significant increase compared with NT control, while WDR KO significantly decreases maximum cell distance. (D) Representative brightfield images of spheroids at day 0 and 11 for each cell line in HA-only gels. (E) Calculated fold area change of day 11 normalized to day 0 area of spheroids. CFL KO shows significant increase compared with NT control, while PFN KO and WDR KO significantly decrease area change. (F) Maximum cell distance from the sphere edge. CFL KO shows significant increase compared with NT control, while PFN KO and WDR KO significantly decrease maximum cell distance. In all graphs, the dashed lines denotes the mean value of NT sgRNA control and error bars represent mean with SD. *P <0.05; ****P < 0.0001 by Kruskal–Wallis test followed by Dunn's multiple comparisons test; scale bar, 100 μm.

not show significant differences in 3D area change in the HA-RGD matrix compared with NT control, while PFN KO and WDR KO had significantly lower 3D area change (Figure 2B). Of note, CAP KO showed both increased area change (Figure 2B) and significantly increased maximum cell distance (Figure 2C), albeit to a lesser extent than CFL KO. Considering that CAP is a cofactor of CFL, this result in tandem with the CFL KO results indicates that attenuating CFL activity increases 3D motility in HA-RGD matrices.

We next asked whether CRISPR KO of these same targets would modulate 3D migration through "bare" HA gels lacking pendant RGD peptides (HA-only), where cells presumably rely on nonintegrin-based adhesion receptors to directly engage the matrix. In an HA matrix, cells can interact with the polysaccharide backbone through membrane receptors such as CD44 and receptor for HA-mediated motility (Toole, 1990; Ponta et al., 2003; Kelly et al., 2024). In the HA-only gels, CFL KO spheres notably were the only ones to invade after 11 d, while all other cells lines displayed minimal protrusion and infiltration into the surrounding matrix (Figure 2D). CFL KO cells had both significantly increased area change and maximum cell distance compared with NT control (Figure 2, E and F). In our past work, bare HA matrices have frequently been restrictive of GBM cell invasion relative to HA-RGD matrices (Wolf et al., 2018; Amofa et al., 2024), so it was remarkable to observe CFL KO cells robustly invading the HA-only gels. Mirroring the HA-RGD results, PFN KO and WDR KO cells had both significantly decreased area change and maximum cell distance compared with control (Figure 2, E and F). Our 3D invasion studies collectively suggest that the loss of PFN and WDR expression inhibit 3D migration, and suppression of CFL activity speeds up 3D migration through HA matrices. Only CFL KO produced appreciable 3D invasion in migration-restrictive HA-only matrices, highlighting a special role for CFL in migration through 3D HA.

CFL KO drives 3D motility by favoring greater actin polymerization in and formation of cellular protrusions.

Extension of cellular protrusions is one of the key steps in the classical cell motility cycle. In 2D, cells frequently extend lamellipodia to advance the leading edge, whereas cells in 3D utilize a large diversity of protrusive mechanisms to advance through the ECM, which vary in their actin-dependence and can change to adapt to the features of a given matrix (Petrie and Yamada, 2012; Caswell and Zech, 2018; Belian et al., 2023). As discussed in the introduction, we previously identified a mechanism through which GBM cells interact with and migrate through 3D HA-matrices using actin- and tubulinbased McTNs (Wolf et al., 2020). In other work, highly metastatic and invasive cancer cell lines had more protrusions per cell and longer protrusion lifetime than less invasive cell lines, which was shown to depend on the LIMK/CFL pathway (Scott et al., 2010; Shibue et al., 2013). During invasion through the ECM, actin polymerization provides the necessary force for these cellular protrusions to penetrate through steric barriers within the matrix (Wyckoff et al., 2006). As the proteins in our CRISPR screen have key roles in actin turnover, we asked whether KO of our target proteins would affect cell protrusion phenotype, with special interest in determining whether CFL KO, which sped up 3D invasion, would also stimulate protrusions. To quantify and compare protrusion phenotype across the cell lines, we used a protrusion formation assay developed in our previous study (Wolf et al., 2020) in which we seeded single cells into 3D HA-only and -RGD gels and let the cells form protrusions for 4 d before fixing and staining with phalloidin. Using z-stack maximum projections of F-actin-stained cells, we quantified the number and maximum length of protrusions per cell (Figure 3,

A-D). In both HA-only and -RGD gels, CFL KO cells had the longest and most protrusions per cell, implying that CFL suppression most strongly favored actin polymerization in the protrusions (Figure 3, C, B, E, and F). Thus, loss of CFL promotes these actin-based protrusions, suggesting that these protrusions may faciliate 3D migration through the HA matrix.

CFL KD confirms 2D motility phenotype from CRISPR

We next sought to gain additional mechanistic insight into the role of CFL KO in driving faster 3D motility. Although the CRISPR KO system allowed us to efficiently screen multiple targets in parallel, we did not perform clonal selection and therefore were working with a heterogeneous population of edited cells. To introduce a more homogeneous and completely independent system for CFL suppression, we transduced U251 cells with two shRNAs (Figure 4), both of which reduced CFL expression by >90% relative to controls (Figure 4, A and B). Targeted KD of CFL did not alter expression levels of actin depolymerization factor (ADF, also known as destrin), the other cofilin isoform expressed in nonmuscle cells (Supplemental Figure S1), similar to previous studies from our laboratory (Lee and Kumar, 2020). Cofilin-2, the third cofilin isoform, is restricted to skeletal muscle and was therefore not considered in this study.

CFL KD cells had aberrant morphologies compared with NT controls on both fibronectin-coated glass and 2D HA-RGD substrates (Figure 4C). CFL KD cells also exhibited less pronounced front-back polarity marked by multiple small lamellipodia (Figure 4, C, D, and G) matching the morphological changes described in our previous study (Lee and Kumar, 2020). Furthermore, CFL KD cells migrated less persistently than NT controls in 2D single cell random migration assays on 2D tissue culture plastic and 2D HA-RGD gels (Figure 4, F-I). Throughout the migration assay, CFL KD cells produced multiple lamellipodia but failed to establish a dominant leading edge or migrate persistently (Figure 4, D and G), consistent with previous work (Hotulainen et al., 2005; Lee and Kumar, 2020). Although neither CFL KD1 nor KD2 showed significantly reduced cell speed on tissue culture plastic (Figure 4E), CFL KD1 did show a significant decrease in cell speed compared with NT control on HA-RGD (Figure 4H).

CFL KD accelerates 3D motility through HA matrices

To validate our findings from the CRISPR screen of the effects of cofilin depletion on 3D motility, we conducted 3D spheroid invasion assays in HA-only and -RGD gels as described previously. Consistent with CFL KO results from our initial screen, CFL KD cells had significantly increased area change and maximum cell distance after 4 d of invasion in HA-RGD gels compared with NT control cells (Figure 5, A-C). Likewise, after 11 d in the HA-only gels, CFL KD cells readily migrated through the matrix, with increased area change and maximum cell distance relative to control, signifying that loss of CFL activity through CRISPR-Cas9 KO or shRNA phenocopied one another (Figure 5, D-F). The NT control cells in the HA-only gels behaved similarly to the NT and NC sgRNA control cells in that they displayed little to no penetration of the surrounding matrix and only exhibited short protrusions at the end of the assay (Figure 5D).

We additionally quantified the instantaneous speeds of invading cells using timelapse imaging to query whether increased cell speeds or persistence were contributing to the increased invasion of the matrix seen in CFL KD cells. We chose to quantify invasion speeds only in HA-RGD gels as NT cells did not show appreciable invasion in HA-only gels. Over a period of 6 h on day 4 of the

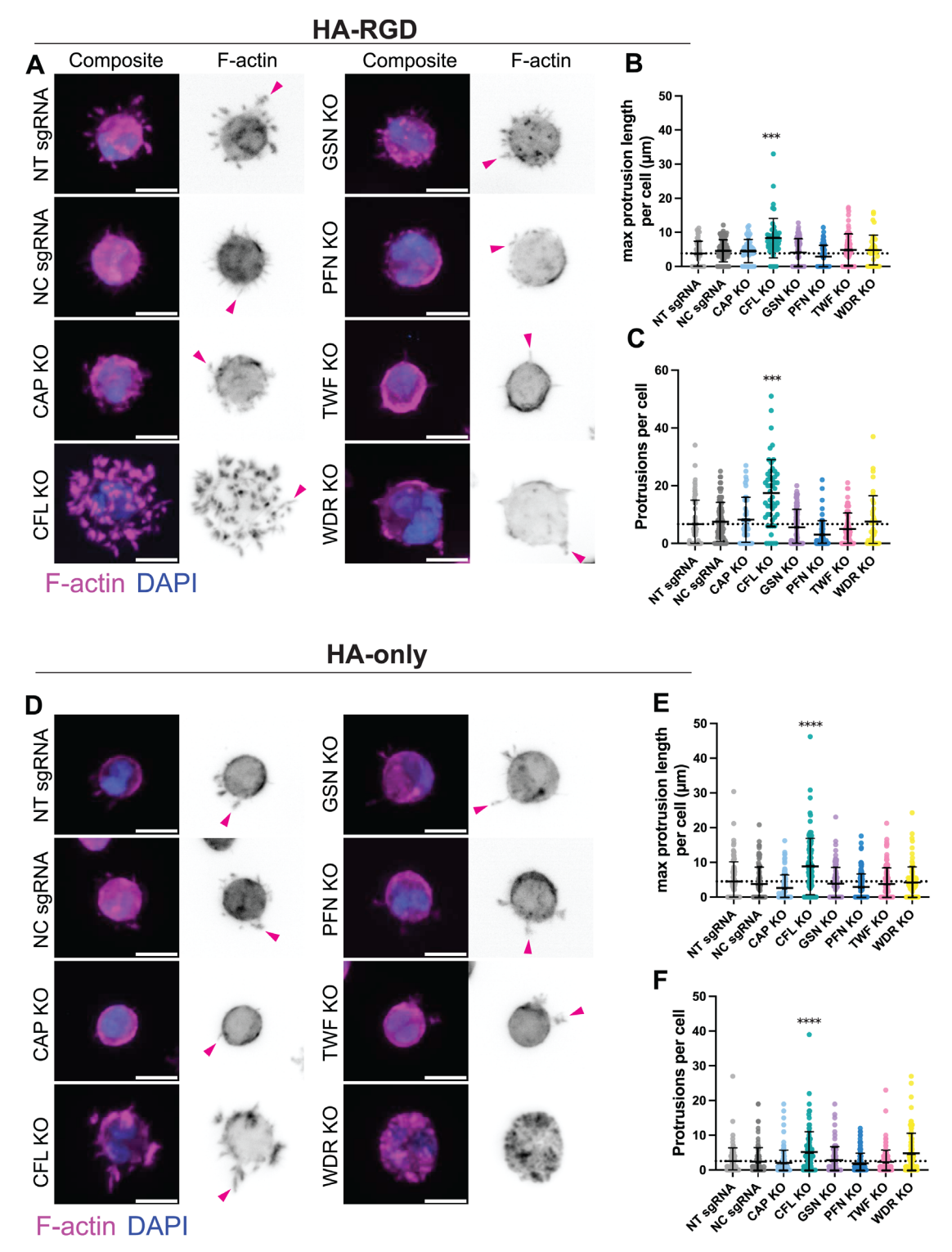


FIGURE 3: 3D protrusion formation assay of CRISPR KO cells in HA gels. Cells were allowed to form protrusions for 4 d before fixation and analysis. (A) Representative images of cells in HA-RGD gels. In the composite image, magenta is F-actin, blue is DAPI, while the inverted image to the right shows F-actin only. The pink triangles on the inverted image denote the longest protrusion for each displayed cell. (B) Number of protrusions per cell. CFL KO has significantly increased protrusion numbers compared with NT control. (C) Maximum protrusion length per cell. CFL KO shows significantly longer protrusions than NT control. (D) Representative images of cells in HA-only gels. In the composite image, magenta is F-actin, blue is DAPI while the inverted image to the right shows F-actin only. The pink triangles on the inverted image denote the longest protrusion for each displayed cell. (E) Number of protrusions per cell. CFL KO has significantly increased protrusion numbers compared with NT control. (F) Maximum protrusion length per cell. CFL KO shows significantly longer protrusions than NT control. In all graphs, error bars represent mean with SD. ***P < 0.001; ****P < 0.0001 by Kruskal–Wallis test followed by Dunn's multiple comparisons test; scale bar, 20 µm.

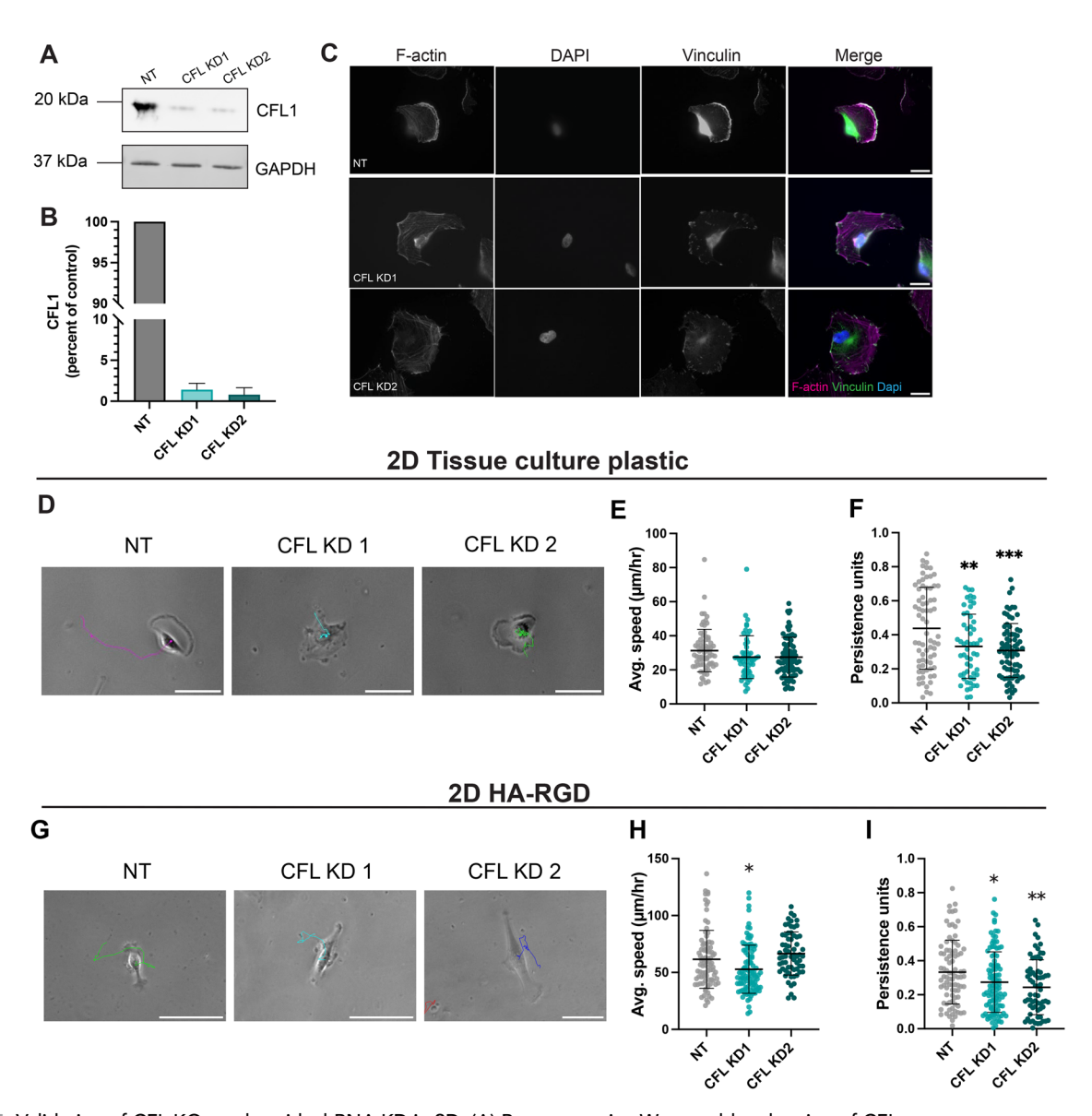


FIGURE 4: Validation of CFL KO results with shRNA KD in 2D. (A) Representative Western blot showing of CFL expression with NT and CFL KD cell lines, where efficient reduction of CFL expression was achieved with shRNA KD. CFL KD1 and CFL KD2 were cell lines transfected with different shRNA constructs, while NT was transfected with an NT shRNA. (B) Quantification of three independent blots with densitometry. Both CFL KD1 and KD2 express <5% of CFL1 protein level of NT control. (C) Representative images of cells cultured on fibronectin-coated glass, stained via IF for F-actin and vinculin. CFL KD results in disorganized lamellipodia and an accumulation of actin filaments; scale bar, 20 μm. (D) Representative brightfield images of cells during random single migration assays on tissue culture plastic. The colored line represents the migration track of the cell over 25 points and 4.2 h, with 10 min between each point. CFL KD cells had little directional migration and displayed multiple lamellipodia; scale bar, 40 µm. (E) CFL KD did not decrease cell speed compared with NT control. (F) CFL KD cells migrated with significantly less persistence than NT control. (G) Representative brightfield images of cells during random single migration assays on 2D HA-RGD gels. The colored lines represent the migration track of the cell over 25 points and 4.2 h, with 10 min between each point. CFL KD cells had little directional migration and displayed multiple lamellipodia; scale bar, 40 µm. (H) Only CFL KD1 showed significantly decreased cell speed compared with NT control. (I) CFL KD cells migrated with significantly less persistence than NT control. In all graphs, error bars represent mean with SD. *P < 0.05; **P < 0.01; ***P < 0.001 by Kruskal-Wallis test followed by Dunn's multiple comparisons test.

invasion assay, CFL KD cells were significantly more persistent but did not have significantly different cell speed compared with NT control (Supplemental Figure S2). This mirrors what we observed with CFL KD cells in 2D motility, where CFL KD cells were significantly less persistent with no significant differences in cell speed (Figure 4I).

Contributions of CFL to invasion is specific to 3D HA matrices

Although the preceding results demonstrate that CFL suppression enhances 3D motility, there are multiple hypothetical explanations for how this might occur. In a previous study, we demonstrated that KD of LIMK1/2—which increases CFL activation—reduced

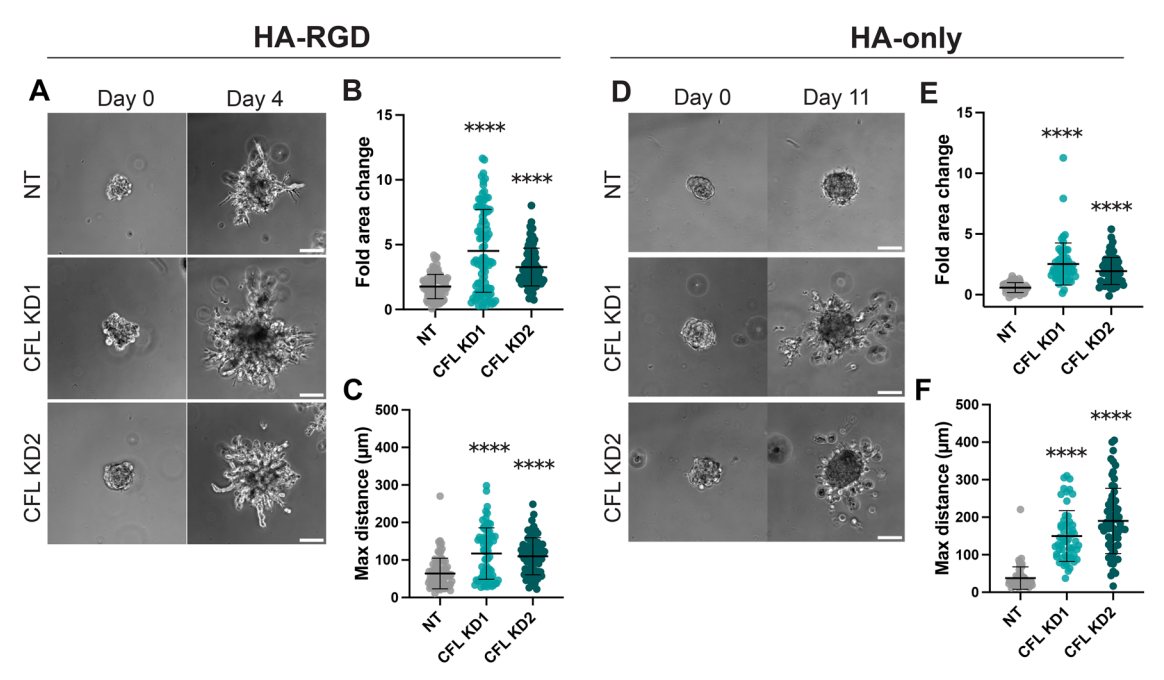


FIGURE 5: Validation of CFL KO results with shRNA KD in 3D. (A) Representative brightfield images of spheroids at day 0 and 4 for each cell line in soft HA-RGD gels. (B) Calculated fold area change of day 4 normalized to day 0 area of spheroids. CFL KD1 and KD2 show significant increase compared with NT control. (C) Maximum cell distance from the sphere edge. Both CFL KD lines show significant increase compared with NT control. (D) Representative brightfield images of spheroids at day 0 and 11 for each cell line in HA-only gels. (E) Calculated fold area change of day 11 normalized to day 0 area of spheroids. Both CFL KD cell lines show significantly increased area change compared with NT control. (F) Maximum cell distance from the sphere edge. Both CFL KD cell lines show a significant increase compared with NT control. In all graphs, error bars represent mean with SD. ****P < 0.0001 by Kruskal–Wallis test followed by Dunn's multiple comparisons test; scale bar, 100 μm.

invasion by impairing the ability of GBM cells to navigate confined environments (Chen et al., 2020). This raises the possibility that CFL suppression might increase motility speed by enhancing the ability to traverse confined spaces inherent in 3D ECMs. To address this possibility in a way that isolates confinement, we conducted Boyden chamber (transwell) invasion assays with 8 µm diameter pores and HA-only coating. After 4 h of invasion, there was no significant difference of percentage of cells that migrated through the membrane of the well inserts between NT and CFL KD1 and 2, perhaps, indicating that confined migration is not a key driver in the increase in 3D motility (Figure 6A). Next, we queried whether directional migration cues from cell-cell contacts or chemotactic gradients played a role in the phenotype we observed. To address this possibility in an isolated way, we conducted 2D "scatter" assays in which we deposited cell spheroids onto 2D glass and HA-RGD surfaces and tracked cell trajectories as the cells migrated out and escaped from the spheroid. On 2D glass surfaces, CFL KD did not affect cell speed but did increase persistence for CFL KD1 (Figure 6, B and C). Similarly, the persistence of the CFL KD cells were significantly higher than NT control on the HA-RGD gels, but CFL KD1 displayed significantly lower cell speeds (Figure 6, F and G). To facilitate comparisons with the 3D migration studies, we also analyzed the scatter assays using relative area change (Figure 6, D and H) and the furthest cell from sphere core (Figure 6, E and I). For both metrics, CFL KD cells were not significantly different than NT control (Figure 6, D, E, H, and I). As there were minimal differences between NT and CFL KD cells in these reductionist studies, CFL suppression appears most likely to increase motility within 3D HA matrices through promotion of protrusive structures.

To assess whether HA per se is needed to support faster 3D motility with CFL suppression, we conducted a similar spheroid invasion assay in collagen I gels (Figure 6F). After 24 h, only CFL KD1 had significantly increased area change compared with NT control (Figure 6G) and neither CFL KD1 and KD2 had significantly increased maximum distance (Figure 6H). Because invasion through collagen (24 h) is generally much faster than in HA (4–11 d) due to the prominent fibrous contact guidance cues, subtle differences in invasive capacity associated with CFL KD may be lost. The lower steric barriers in collagen may also deemphasize the need for more efficient matrix protrusion. Nonetheless, the absence of a strong enhancement of migration upon CFL KD in collagen suggests specificity of the effect to 3D HA, or at least to nonfibrillar, nanoporous matrices.

Protrusions contain markers of microtentacles and filopodia irrespective of CFL status

In our initial screen (Figure 3), we showed that CFL KO increased the number and length of cellular protrusions. We next asked whether these increased protrusions also compositionally differed from NT. To characterize the protrusions, we used immunofluorescence to probe for McTN and filopodia markers (Bohil et al., 2006; Jacquemet et al., 2015; Wolf et al., 2020). We applied a similar protrusion formation assay as in the CRISPR screen, seeding the cells as single cells into HA-only and HA-RGD gels. For this assay, we allowed the cells to form protrusions for 7 d to ease characterization. In both matrix conditions, we observed that protrusions in both NT and CFL KD cells were all positive for CD44 and HYAL2 (a hyaluronidase ubiquitously expressed by GBM cells)

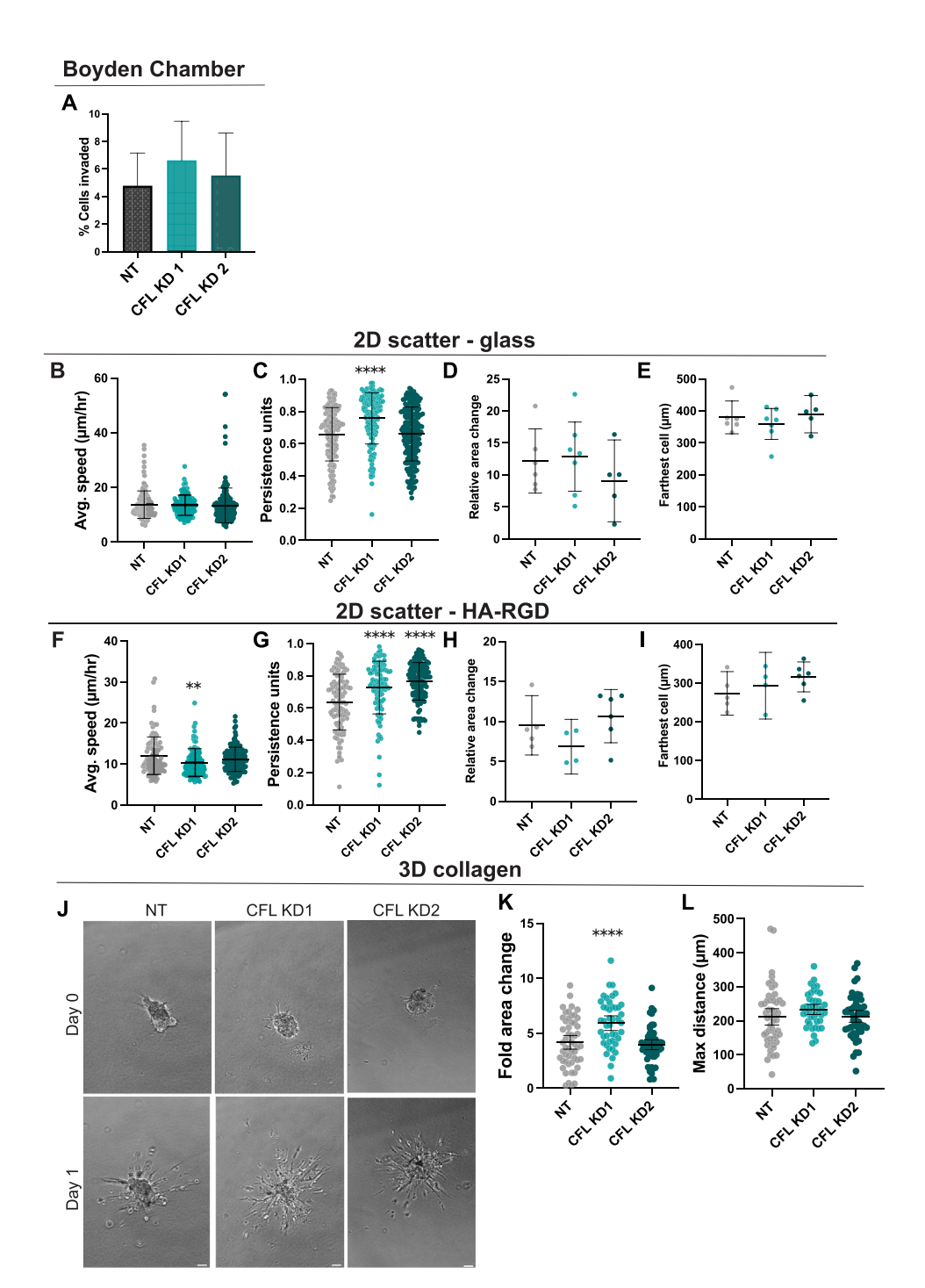


FIGURE 6: Contextualizing the effects of CFL KD on aspects of 3D motility. (A) The percentage of cells invaded through an 8-µm-pore Boyden chamber membrane coated with HA. CFL KD cells did not show a significant increase compared with NT control. Data represent the average of N=5 for each condition. (B–I) 2D spheroid scattering assay. Cells were tracked for 46 points over a period of 7.75 h, with 10 min between each point. B, C, F, and G represent individual cell measurements from 4 to 6 spheres, with each sphere being an independent biological replicate. D, E, H, and I represent the measurements of each sphere at the end of the assay. (B and C) On glass, when compared with NT control cells, CFL KD cells did not show significantly different speeds, but CFL KD1 exhibited significantly higher persistence. (D and E) The relative area change and farthest cell were not significantly different between CFL KD cells and NT control. (F and G) On 2D HA-RGD, only CFL KD1 cells had significantly reduced speeds, but both CFL KD1 and KD2 cells had significantly increased persistence compared with NT control. (H and I) The relative area change and farthest cell were not significantly different between CFL KD cells and NT control. (J-L) 3D collagen invasion assay. (J) Representative brightfield images of spheroids at day 0 and 1 for each cell line in collagen gels. (K) Calculated fold area change of day 1 normalized to day 0 area of spheroids. Only CFL KD1 spheres show significant increase compared with NT control; scale bar, 100 µm. (L) Maximum cell distance from the sphere edge. CFL KD cells did not show a significant increase compared with NT control. In all graphs, error bars represent mean with SD. **P < 0.01; ****P < 0.0001 by Kruskal-Wallis test followed by Dunn's multiple comparisons test.

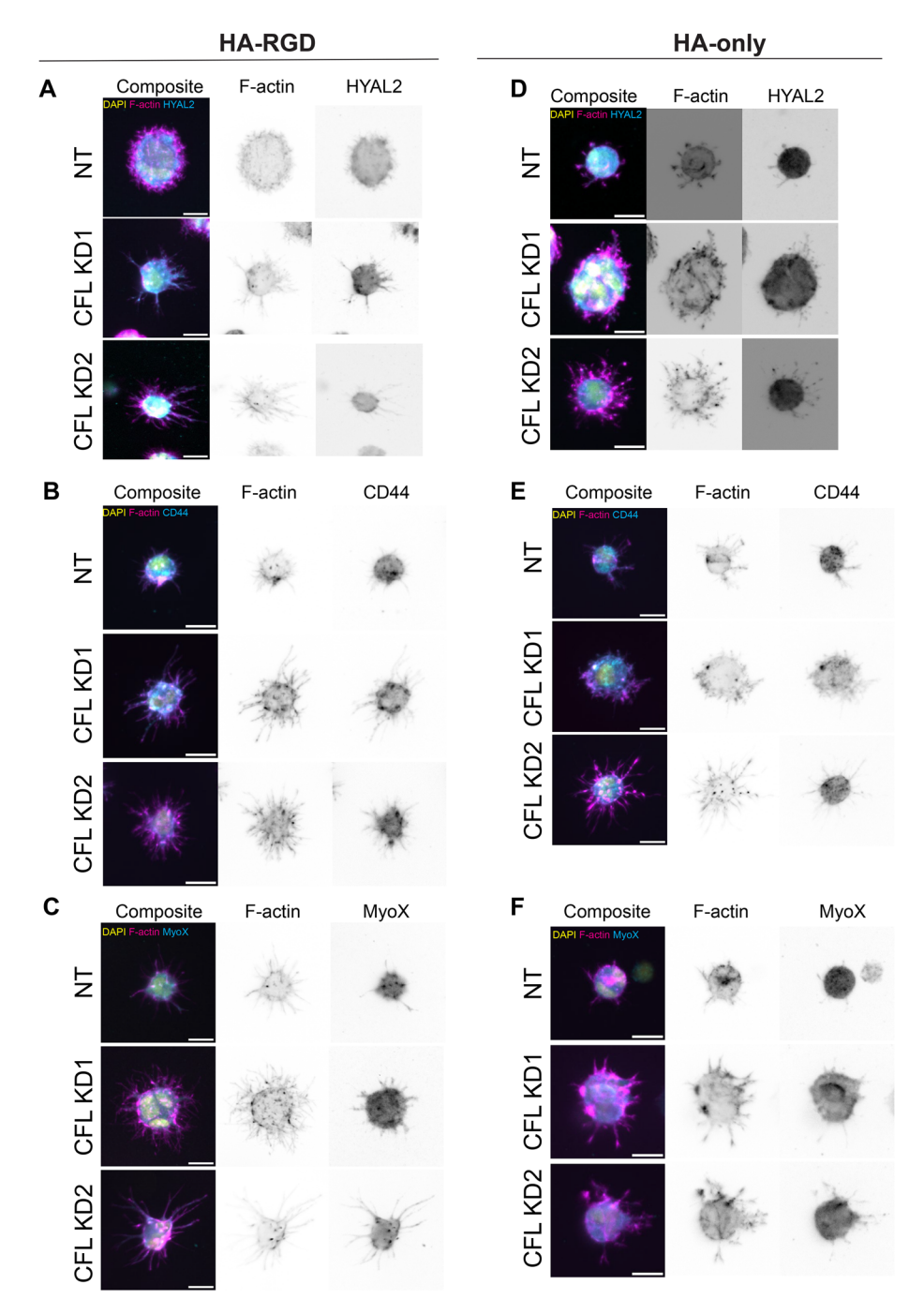


FIGURE 7: Cells in the HA matrices display F-actin-based protrusions with both McTN and filopodial markers. Representative images of single cells encapsulated within HA-only and HA-RGD 3D gels, which were allowed to form protrusions for 7 d. The images represent 3 independent replicates with roughly 30 cells per condition. (A and D) Most protrusions are positive for HYAL2, indicating HA matrix-degradation capabilities. (B and E) Most protrusions are also CD44-positive and thus can interact with the surrounding matrix. (C and F) Protrusions show heterogeneous expression of MyoX, with cells in HA-RGD having more MyoX-positive protrusions than in HA-only. In all composite images, yellow is DAPI, magenta is F-actin, and cyan represented the marker being probed for; scale bar, 20µm.

(Figure 7, A, B, D, and E), implying that the protrusions could adhere to and degrade the HA matrix, like our previous description of McTNs and reminiscent of invadopodia and MMPs in other contexts. Both NT and CFL KD protrusions in the HA-only matrix displayed minimal expression of the canocial filopodial marker myosin 10 (Myo X), indicating that these protrusions share more functional similarities to McTNs than to filopodia (Figure 7C). In the HA-RGD

matrix, all cells displayed heterogeneous expression of Myo X in protrusions (Figure 7F). Cells that had shorter or fewer protrusions displayed little to no Myo X-positive protrusions, while cells that had longer and or more protrusions had many Myo X-positive protrusions. This observation indicates that in the 3D HA-RGD matrix, the protrusions display a mix of McTN and filopodial characteristics. These observations were also seen in invading spheroids. We

observed that in spheroids that were allowed to invade for 4 d in 3D HA-RGD matrices, for both NT and CFL KD cells, protrusions of cells along the invasive front were all positive for CD44 and HYAL2. The invasive cells also displayed protrusions with heterogeneous expression of MyoX (Supplemental Figure S3, B-D). Thus, although CFL KD increases protrusion number and length, it does not appear to fundamentally change protrusion composition.

DISCUSSION

It is unclear how the systems the regulate actin turnover that have been broadly characterized in 2D operate in 3D migration (Petrie and Yamada, 2012; Doyle et al., 2013), particularly in defined, nonfibrillar matrices such as HA. In this study, we investigated contributions of the actin turnover machinery to 3D invasion of GBM cells through HA. Our CRISPR KO screen of core actin turnover proteins revealed that only CFL suppression produced differential effects in 2D and 3D motility, slowing motility in 2D and increasing it in 3D. Additionally, CFL KO cells were distinct among screened candidates in forming longer and more actin-based protrusions per cell, hinting at a role of actin polymerization and stabilization in faster 3D migration. We independently confirmed this result with targeted shRNA KD and could not recapitulate the result in 3D collagen or transwell invasion assays, pointing to the specificity of this result to migration through 3D HA, or at least a nanoporous, nonfibrillar matrix. Mechanistic studies revealed that protrusions seen in the setting of CFL suppression include F-actin along with both McTN and filopodial markers. Our data support a model in which attenuated CFL activity promotes actin polymerization within a variety of protrusions and enhances the ability of GBM cells to migrate through HA.

How the components involved in actin turnover, including the LIMK/CFL pathway, contribute mechanistically to cell motility varies with matrix context (Caswell and Zech, 2018). In 2D, attenuating CFL expression and activity, either directly or through LIMK overexpression, altered lamellipodial actin networks and decreased directional motility (Zebda et al., 2000; Sahai et al., 2001; Hotulainen et al., 2005; Wang et al., 2006; Nagai et al., 2011; Lee and Kumar, 2020). Reciprocally, overexpression of WT CFL and constitutively active CFL mutants enhanced the motility of GBM cells (Yap et al., 2005; Nagai et al., 2011). However, diminishing LIMK expression or activity and increasing the amount of activated CFL was shown to negatively affect 2D motility in chemokine-stimulated migration (Nishita et al., 2005; Kobayashi et al., 2006; Horita et al., 2008). This dichotomy is also seen in 3D cell motility and cancer invasion, in that CFL and its regulators are seen as both positive and negative factors in migration. Diminished CFL expression reduced motility of T cells in collagen and Matrigel (Klemke et al., 2010; Salz et al., 2020) and invasion of tumor cells in transwell assays (Horita et al., 2008; Nagai et al., 2011). Although in our study, attenuating CFL activity increases motility speed through 3D HA.

The relationship between CFL activity and 3D migration has proven surprisingly complex, with the end effect depending on the biological system and method of perturbation. Suppression of CFL activators chronophin (CIN) and slingshot 1 and 2 (SSH) might be expected to decrease CFL activation but appears to impact migration in different ways. SSH KD decreased the invasive capability of T cells and hepatoma cells (Nishita et al., 2005; Horita et al., 2008), while CIN KD increased the in vitro invasive capability of GBM cells (Schulze et al., 2016). LIMK inhibition has been shown to slow cancer cell migration and invasion in both in vitro and in vivo studies by disinhibiting CFL (Yoshioka et al., 2003; Ding et al., 2008; Scott

et al., 2010; Chen et al., 2020; Wang et al., 2021). It is possible that CFL activity is tuned to some strongly context-dependent optimum (Wang et al., 2006; 2007). This idea is consistent with the observation that LIMK/CFL pathway expression and activity varies with cell type (Shishkin et al., 2016; Coumans et al., 2018) and the fact that 3D migratory mode is strongly regulated by matrix properties (Friedl et al., 2012; Yamada and Sixt, 2019; Tran and Kumar, 2021). If an optimum indeed exists, the differential effect of CFL suppression on 2D versus 3D migration suggests that this value depends strongly on matrix dimensionality, with greater actin polyermization needed to overcome steric barriers inherent to nanoporous 3D matrices.

Previous work has shown that actin-rich protrusions in a 3D matrix have been used for adhesion to and penetration through the matrix (Shibue et al., 2013; Jacquemet et al., 2015; Caswell and Zech, 2018; Wolf et al., 2020). These studies share a common mechanism in which F-actin stability supports protrusion formation and extension through the ECM (Caswell and Zech, 2018). In one study, highly metastatic tumor cells produced more and longerlived filopodial protrusions than less aggressive tumor cells. This phenotype depended on LIMK-mediated CFL inactivation, with diminished CFL activity stabilizing F-actin within the protrusions (Shibue et al., 2013), consistent with our results. The LIMK/CFL signaling pathway has also been implicated in the maturation of invadopodia for matrix degradation. Increased CFL activity decreased F-actin stability within the invadopodia, thereby inhibiting matrix degradation via matrix-metalloproteinases and decreasing 3D motility (Yamaguchi et al., 2005; Oser et al., 2009; Scott et al., 2010). The protrusions in our study express HYAL2, implicating that these protrusions are also involved in HA degradation and thus permit GBM cell invasion, mirroring the role of invadopodia and matrix-metalloproteinases in 3D motility.

Although all the proteins screened in this study are important regulators of actin turnover, CFL KO was the only condition to significantly increase 3D motility and did so to a much larger degree than control cells. We attribute this result to the primary role of CFL in enhancing actin turnover. In cells, the enhanced actin filament turnover and depolymerization is attributed to CFL activity (Bamburg, 1999; McGrath et al., 2000; Southwick, 2000). Although other proteins in the screen do display actin filament-severing functions, like GSN and TWF, they also play distinctly different functions than CFL in the actin turnover machinery (Southwick, 2000; Hilton et al., 2018; Kotila et al., 2019; Colin et al., 2023). KO of CFL may have had the strongest effect on actin turnover, therefore resulting in the biggest change in 3D motility. It would be fruitful to repeat these studies in other cell types and matrix conditions that support 3D migration through actindependent but non-filopodial/microtentacle-based mechanisms to query whether CFL has similar contributions to those modes of motility.

Using a defined and engineered hydrogel platform, we were able to dissect the contributions of CFL to GBM cell motility through 3D HA matrices. We demonstrated that suppression of CFL increased both the length and number of protrusions to speed up 3D motility. In future studies, it would also be valuable to capture the dynamics of the protrusions observed in this study at high spatial and temporal resolution during 3D migration, ideally taking advantage of superresolution tools and new reagents for localized modulation of CFL in subcellular compartments (Stone et al., 2019). Although we showed that the differential effect of CFL suppression holds in HA but not collagen I, it will be important in the future to explore a much wider range of matrix types exhibiting a diversity

of adhesive, microstructural, and mechanical properties. Additional studies in organotypic models (e.g., brain slice culture) should also complement and lend new mechanistic insight into the wealth of studies focused on the role of CFL in migration in vivo, especially those focused on the role of CFL in motility within tissue (Wang et al., 2006; 2017; Nagai et al., 2011; Bravo-Cordero et al., 2013; Shibue et al., 2013). Our work provides insight into the contributions of CFL and actin turnover within protrusions and 3D motility and opens new mechanistic questions to explore.

MATERIALS AND METHODS

All key resources used are listed Supplemental Table S1.

Cell culture

U-251 MG human GBM (U251) cells were obtained from the University of California, Berkeley Tissue Culture Facility. The cells were cultured in DMEM (Gibco) supplemented with 10% (v/v) FBS (JR Scientific), 1% (v/v) nonessential amino acids (Gibco), 1% (v/v) sodium pyruvate (Thermo Fisher Scientific), and 1% (v/v) penicillin/streptomycin (Gibco). Cells were passaged every $\sim 7~\rm d$ with media changes every other day and harvested using 0.25% trypsin-EDTA (Thermo Fisher Scientific). Cells were passaged less than 30 times and were screened every 3 mo for *Myocoplasma*. All U251 cells transduced with shRNA or sgRNA expression plasmids were maintained in 1 µg/ml puromycin (Clontech). U251 cells transduced with Cas9 and sgRNA expression plasmids were additionally maintained in 10 µg/ml blasticidin (Invivogen).

CRISPR KO cell line generation

Cas9 and sgRNA expression vectors were stably introduced to U251 cells using methods described previously (McCollum et al., 2023). Briefly, the lentiCas9-blast plasmid (Addgene, 52962) was transfected into HEK 293T cells (provided by David Schaffer's laboratory at UC Berkeley, originally sourced from ATCC Cat# CRL-11268, CVCL_1926) using third-generation lentiviral packaging plasmids (pMD2.G, Addgene, 12259; pMDLg/pRRE, Addgene, 12251; pRSV-Rev, Addgene 12253) using PolyJet reagent (Signa-Gen) (Dull et al., 1998; Sanjana et al., 2014). The supernatant was harvested at 48 h and 72 h posttransfection and syringe filtered through a 0.45-µm pore-sized filter (Millipore) and then pooled. The filtered supernatant was used to transduce U251 cells at a multiplicity of infection (MOI) of 1 with 10 µg/ml polybrene. After 48 h posttransduction, cells were selected using 10 µg/ml blasticidin for 2 wk for Cas9 integration.

For each protein target in the KO array, three separate guides targeting the gene were generated using CRISPick (Broad Institute). Three NC and NT guides were used as controls and have been previously published (Morgens et al., 2017). Oligos for each guide sequence (Elim Biopharma) with the appropriate overhangs were annealed and ligated into pMCB320 (Addgene 89359) digested with BstXI and BlpI (New England Biolabs) using T4 DNA ligase (New England Biolabs) (Han et al., 2017). All sqRNA sequences used in this study are listed in Supplemental Table S2. The sgRNA plasmids for the same genetic target were pooled together in proportional amounts and transfected with third-generation lentiviral packaging plasmids into HEK293Ts using PolyJet. At 48 and 72 h posttransfection, the supernatant was harvested and filtered and pooled together. The filtered supernatant was used to transduce Cas9 U251 cells at a MOI of 2 with 10 µg/ml polybrene. Cells were maintained in 10 µg/ml blasticidin and 2 µg/ml puromycin starting at 48 h posttransduction to select for sgRNA integration and expanded 7 d post-transduction. pMD2.G, pMDLg/pRRE, pRSV-Rev, pMCB320, and lentiCas9-Blast were provided by Britt Glaunsinger's laboratory at UC Berkeley and were originally sourced from Addgene. pMCB320, lentiCas9-Blast, and lentiviral packaging plasmids (pMD2.G, pMDLg/pRRE, pRSV-Rev) were originally developed in the laboratories of Michael Bassik Feng Zhang, and Didier Trono, respectively.

CFL shRNA KD cell line generation

U251 CFL shRNA KD cells were generated using methods as described previously (Lee and Kumar, 2020). Briefly, shRNA constructs targeting the human CFL isoform (CFL KD1: 5'-ACGACATGAGGTGCGTAAGT-3', CFL KD2: 5'-AAGGAGGATCTGGTGTTTATC-3') and an NT sequence (NT: 5'-GCTTCTAGCCAGTTACGTACA-3') were cloned into the pLKO.1-TRC cloning vector (Addgene, 10878) using Agel and EcoRI (Moffat et al., 2006). pLKO.1-TRC was orginally developed in the laboratory of David Root. Lentivirus particles were produced using HEK 293T cells using second-generation packaging plasmids (pMD2.G; psPAX2, Addgene, 12260) for each construct. U251 cells were transduced with shRNA viral particles at a MOI of 1. After 48 h posttransduction, cells were selected using 2 µg/ml puromycin for 1 wk for shRNA integration. KD efficiency was assessed via Western blot.

Generation of spheroids

U251 cell spheroids were generated using AggreWell 400 plates (STEMCELL Technologies). Briefly, the wells of the AggreWell plate were incubated with an anti-adherence rinsing solution (STEMCELL Technologies) then washed with fresh media. U251 cells were seeded as single cells at a density of $\sim\!\!3\times10^5$ cells per well. Cells were allowed to grow and aggregate into spheres for 4 d. The spheres were then harvested and used for assays.

HA synthesis and RGD conjugation

HA hydrogels were fabricated as described previously (Ananthanarayanan et al., 2011; Wolf et al., 2020). Briefly, sodium hyaluronate (Lifecore Biomedical, Research Grade, 66–99 kDa) was functionalized with methacrylic anhydride (Sigma-Aldrich, 94%) to synthesize methacrylated HA (HA-Me). The extent of methacrylation per disaccharide was quantified with ¹H NMR as described previously and calculated to be ~85% for the HA-Me used in this study (Ananthanarayanan et al., 2011). To add integrin-binding motifs, HA-Me was conjugated with RGD peptide Ac-GCGYGRGDSPG-NH2 (Anaspec) at a concentration of 0.5 mmol/L via Michael Addition. Cross-linker details are described in the 2D gel fabrication and 3D spheroid encapsulation sections below.

2D gel fabrication

Before gel fabrication, glass-bottom plates were coated with 1mg/ml poly-d-lysine solution (Sigma-Aldrich) and rinsed with 1x PBS (Fisher BioReagent) to enable gel adsorption to the glass. Phenol-free DMEM (Thermo Fisher Scientific) and HA-RGD solution at 6% (w/w) stock were mixed to generate a final concentration of HA-RGD of 5% (w/w). Bifunctional thiol dithiothreitol at 5% (w/w) stock (DTT, Thermo Fisher Scientific) was then added at thiol:HA monomer repeat (T:M) ratio of $\sim\!0.4$ to achieve a shear modulus of $\sim\!6.5$ kPa. The solution was plated at 6 μ l per gel into the treated glass-bottom plates, then flattened with a plasma-treated glass coverslip, creating flat gels of $\sim\!120~\mu m$ in height. The flattened gels were incubated for 1 h in a humidified 37°C chamber. Once

the gels were cross-linked, the coverslips were removed and the gels were soaked in room temperature PBS overnight before cell seeding.

2D migration assay

Before seeding, U251 cells were incubated with SPY555-DNA (Cytoskeleton) at a final concentration of 1:1000 dilution for 24 h to visualize the nucleus. For single cell migration, cells were seeded onto tissue culture plate wells or HA-RGD gels at a density of 1000 cells/cm². For spheroid spreading migration, spheres were collected and seeded onto HA-Me-coated glass or HA gels at a density of 1 to 2 spheres per 12-mm-diameter well. Cells were allowed to spread and attach for 4 h. Afterwards, the cells were imaged every 10 min for 6 h in brightfield and TRITC using a 10x phase objective on an Eclipse TE2000 Nikon microscope and NIS-Elements Software in a humidified 37°C, 5% CO₂ chamber. The ImageJ/FIJI plugin TrackMate was used to track cell movements between each frame and calculate average cell speed and persistence (Schindelin et al., 2012; Tinevez et al., 2017; Ershov et al., 2022).

Spheroid encapsulation in HA

Spheroids were harvested from AggreWell plates and suspended into an HA-RGD or HA-only solution of a final concentration of 1.5% (w/w) with a final density of \sim 625 spheres/ml. Protease-degradable peptide cross-linker with a bifunctional cystine peptide at 10% (w/w) stock (KKCGGPQGIWGQGCKK, Genscript) was then added at a T:M ratio of \sim 0.24 to generate a shear modulus of \sim 300 Pa. The mixture was plated as 8 µl droplets into a nontissue culturetreated plate. The plate was incubated for a total of 1 h in a humidified 37°C with 5% CO₂ chamber with rotation during the first 10 min to ensure that the spheres would stay in the center of the gels, then left upside-down for the remainder of the hour. After gelation, fresh cell culture media were added to the wells to fully submerge the gels. Over the duration of the assay, the media were changed every 2 to 3 d.

Spheroid encapsulation in collagen

Spheroids were harvested from AggreWell plates and suspended into a gel precursor solution composed of bovine collagen type I solution (Advanced Biomatrix), 1N NaOH (Thermo Fisher Scientific), and 1 N HEPES (Life Technologies) to generate a 2 mg/ml final collagen concentration with a density of \sim 625 spheres/ml. The mixture was then plated as 5 µl droplets into a nontissue culturetreated plate that was treated with 1mg/ml poly-d-lysine solution. The plate was incubated for a total of 1 h in a humidified 37°C chamber with 5% CO₂, with rotation during the first 10 min to ensure that the spheres would stay in the center of the gels, then left upside-down for the remainder of the hour. After gelation, fresh cell culture media were added to the wells to fully submerge the gels.

Invasion assay imaging and quantification

Spheroids were tracked for 4 d in HA-RGD, 11 d in HA-only, and 24 h in collagen using a Plan Fluor Ph1 10x phase objective on an Eclipse TE2000 Nikon microscope. Spheres within the gel were randomly selected for imaging, with spheres adhered to the bottom of the plate or near the outer edge or surface of the gel excluded from analysis. NIS-Elements Software was used to acquire images. Invasion was quantified using ImageJ by tracing the outermost edge of the spheroid, including any single cells, on day 0 and the corresponding assay end day (day 4 for HA-RGD, day 11 for in HA-only,

and 24 h for collagen) and calculating the area. The difference between the area of the assay end day and day 0 was then normalized to the day 0 area and reported as relative change in spheroid area. Any spheroids that had a calculated decrease in spheroid area on the assay end day were excluded from analysis. The distance of the farthest cell from the core of the sphere on the assay end day was measured using ImageJ and reported as maximum distance from core sphere edge. We measured maximum cell distance in addition to spheroid area change to account for any contributions of proliferation and cell death to the area change measurement.

For live cell timelapse tracking, spheroids in HA-RGD gels were imaged every 10 min for 6 h on day 4 of invasion. At each timepoint, a z-stack of 30 slices, 5 µm apart, was acquired for each sphere. Cell movements between each frame was tracked using the ImageJ Manual Tracking plug-in and speed and persistence for individual cells were calculated using the tracks.

Boyden chanmber (transwell) assay

Boyden chamber (transwell) inserts with pore sizes of 8 µm (Sterlitech), were incubated with 1.5% (w/w) HA-me diluted in PBS overnight at 4°C, then rinsed three times with PBS. Cells were seeded into the top of each insert at a density of 28k cells/cm² in media containing 1% FBS. The bottom chamber was filled with media containing 10% FBS to create a chemotactic gradient. Cells were allowed to migrate for 4 h, then fixed with 4% paraformaldehyde for 10 min and washed three times with PBS. The cells were permeabilized with 0.5% Triton-X for 10 min and then stained with DAPI (Sigma-Aldrich) for 10 min. The inserts were imaged with an Eclipse TE2000 Nikon microscope and NIS-Elements software. Cell nuclei were counted using a Python-based custom code modified from a previous study (Mohindra et al., 2023).

Immunostaining

All steps were performed at room temperature unless otherwise noted. For 2D samples, before the immunostaining process and between each step, cells were rinsed briefly with PBS. The cells were fixed with 4% (v/v) paraformaldehyde (Alfa-Aesar) for 10 min. Next, the cells were permeabilized with 0.3% (v/v) Triton-X (Sigma-Aldrich) in PBS for 10 min, then blocked with 5% (v/v) goat serum (Thermo Fisher Scientific) in PBS for 1 h. The cells were incubated with primary antibodies for 16 h at 4°C, then incubated with secondary antibodies, phalloidin (647, Cell Signaling Technology; 546, Thermo Fisher Scientific), and DAPI (Sigma-Aldrich) for 1 h. The cells were then mounted using Fluoromount-G (Thermo Fisher Scientific). Samples were imaged within a week of staining.

For 3D samples, before the immunostaining and between each step, cells were rinsed three times with 5 min of shaking in PBS. All incubation steps were performed with shaking. The cells were fixed with 4% (v/v) paraformaldehyde for 15 min. Following, the cells were permeabilized and blocked in a solution of 0.1% (v/v) Triton-X and in PBS with 5% (v/v) goat serum for 40 min. The cells were incubated with primary antibodies for 2 to 3 d at 4°C and then incubated with secondary antibodies, phalloidin, and DAPI for 16 h at 4°C. Stained samples were stored and imaged in 1x PBS. Samples were imaged within a week of staining.

The following primary antibodies were used for immunostaining at a dilution of 1:200: rabbit anti-cofilin (Cell Signaling Technology), mouse anti-vinculin (Sigma-Aldrich), rabbit anti-myosinX (Sigma-Aldrich), rabbit anti-CD44 (Invitrogen), and rabbit anti-HYAL2 (Abcam). The following secondary antibodies were used: Alexa Fluor 488 anti-mouse and Alexa Fluor 647 anti-rabbit, both used at a dilution of 1:500 and from Thermo Fisher Scientific, along with

Alexa Fluor 546 phalloidin (1:300, Thermo Fisher Scientific) and Alexa Fluor 647 (1:30, Cell Signaling Technology) and DAPI (1ng/ μ l, Sigma-Aldrich).

Imaging

For 2D samples, an Eclipse TE2000 Nikon microscope with a 60x objective and a LED lamp were used for epifluorescence imaging. NIS-Elements software was used to acquire the images.

For 3D samples, a Nikon W1 spinning disk confocal with a 10x/0.3NA objective was used for confocal imaging. NIS-Elements software was used to acquire the images. For the 3D images of spheroids for isotype control (Supplemental Figure S3), a Zeiss 980 confocal with a 20x objective was used image the samples with Airyscan confocal imaging. Zeiss Zen microscopy software was used to acquire the images.

Protrusion quantification assay

A z-stack of 250-µm thickness with slices 5 µm apart was acquired in the center of each gel. Each z-stack was then collapsed with a maximum intensity projection for analysis. The ImageJ plug-in SNT was used to trace and measure the length and number of protrusion for each cell in the field of view (Arshadi et al., 2021). Cells that were blurry, too dim, at the edges of the field of view, or were multicellular clumps were excluded from analysis.

Western blot analysis

Cells grown on tissue culture plates were lysed using RIPA buffer (Sigma-Aldrich) supplemented with Halt protease and phosphatase inhibitor cocktail (Thermo Fisher Scientific). Samples were run on a 4 to 12% Bis-Tris gel (Life Technologies), with equal amounts of protein loaded into each lane (~20 µg), then transferred to a nitrocellulose membrane (Licor). For CFL KD verification, membranes were probed with rabbit anti-cofilin antibody (Cell Signaling Technology) and mouse anti-GAPDH (Sigma-Aldrich). To probe for effects of CFL KD on ADF protein levels, membranes were probed with rabbit anti-ADF (AB_476912) and mouse anti-beta actin antibodies (AB_476697). Blots were then probed with the secondary antibodies Alexa Fluor 488 goat antimouse (Thermo Fisher Scientific) or Alexa Fluor 647 goat antirabbit (Thermo Fisher Scientific) for visualization. Primary antibodies were used at a dilution of 1:1000 and secondary antibodies were used at a dilution of 1:10,000. Membranes were imaged using the iBright imaging system (Invitrogen).

Statistical analysis

All graphical representation and statical analysis of the data in this study were performed in GraphPad Prism 10. Unless otherwise noted, data were presented at mean \pm SD. The statical comparisons and details of replicates are described in the figure legends.

DATA AVAILABILITY

The data that support the findings of this study are available from the corresponding author upon reasonable request.

ACKNOWLEDGMENTS

Confocal imaging experiments were conducted at the UC Berkeley Biological Imaging Facility, which was supported in part by the NIH S10 program under Award 1S10OD018136-0, and at the CRL Molecular Imaging Center, RRID:SCR_017852, supported by NIHS10OD025063. We thank Drs. Holly Aaron, Feather Ives, Luis Alvarez, Denise Schichnes, and Caitlin Cornell for technical assis-

tance and training. We also thank the following groups and individuals: Drs. Britt Glaunsinger and Chloe McCollum for providing pMCB230 and plenti-CRISPR plasmids and technical assistance; Dr. David Schaffer for sharing cells and equipment for Western blot; Drs. Bruce Goode and Justin Zhong, as well as all members of the Kumar laboratory for helpful discussion and suggestions. This work was supported by awards from the National Science Foundation (Graduate Research Fellowship; to V.D.T.), the Howard Hughes Medical Institute (HHMI) Gilliam Fellowship and Robert Noyce Memorial Fellowship in Microelectronics (to K.Y.A.), the California Institute of Regenerative Medicine (CIRM) Training program (EDUC4-12790; to L.L.) and the National Institutes of Health (R01CA260443 and R01GM122375 to S.K.). The content is solely the responsibility of the authors and does not necessarily represent the official views of the funding agencies.

REFERENCES

- Amofa KY, Patterson KM, Ortiz J, Kumar S (2024). Dissecting TGF- β -induced glioblastoma invasion with engineered hyaluronic acid hydrogels. APL Bioeng 8, 026125.
- Ananthanarayanan B, Kim Y, Kumar S (2011). Elucidating the mechanobiology of malignant brain tumors using a brain matrix-mimetic hyaluronic acid hydrogel platform. Biomaterials 32, 7913–7923.
- Arshadi C, Günther U, Eddison M, Harrington KIS, Ferreira TA (2021). SNT:
 A unifying toolbox for quantification of neuronal anatomy. Nat Methods
 18. 374–377
- Artym VV, Swatkoski S, Matsumoto K, Campbell CB, Petrie RJ, Dimitriadis EK, Li X, Mueller SC, Bugge TH, Gucek M, et al. (2015). Dense fibrillar collagen is a potent inducer of invadopodia via a specific signaling network. J Cell Biol 208, 331–350.
- Baker BM, Chen CS (2012). Deconstructing the third dimension—how 3D culture microenvironments alter cellular cues. J Cell Sci 125, 3015–3024.
- Balcer HI, Goodman AL, Rodal AA, Smith E, Kugler J, Heuser JE, Goode BL (2003). Coordinated regulation of actin filament turnover by a highmolecular-weight Srv2/CAP complex, cofilin, profilin, and Aip1. Curr Biol 13, 2159–2169.
- Balzer EM, Tong Z, Paul CD, Hung W, Stroka KM, Boggs AE, Martin SS, Konstantopoulos K (2012). Physical confinement alters tumor cell adhesion and migration phenotypes. FASEB J 26, 4045–4056.
- Bamburg, JR (1999). Proteins of the ADF/cofilin family: Essential regulators of actin dynamics. Annu Rev Cell Dev Biol 15, 185–230.
- Bangasser BL, Shamsan GA, Chan CE, Opoku KN, Tüzel E, Schlichtmann BW, Kasim JA, Fuller BJ, McCullough BR, Rosenfeld SS, et al. (2017). Shifting the optimal stiffness for cell migration. Nat Commun 8, 15313.
- Belian S, Korenkova O, Zurzolo C (2023). Actin-based protrusions at a glance. J Cell Sci 136, jcs261156.
- Bellail AC, Hunter SB, Brat DJ, Tan C, Van Meir EG (2004). Microregional extracellular matrix heterogeneity in brain modulates glioma cell invasion. Int J Biochem Cell Biol 36, 1046–1069.
- Bohil AB, Robertson BW, Cheney RE (2006). Myosin-X is a molecular motor that functions in filopodia formation. Proc Natl Acad Sci USA 103, 12411–12416
- Bravo-Cordero JJ, Magalhaes MAO, Eddy RJ, Hodgson L, Condeelis J (2013). Functions of cofilin in cell locomotion and invasion. Nat Rev Mol Cell Biol 14, 405–417.
- Carey SP, Rahman A, Kraning-Rush CM, Romero B, Somasegar S, Torre OM, Williams RM, Reinhart-King CA (2015). Comparative mechanisms of cancer cell migration through 3D matrix and physiological microtracks. APSselect 2, C436–C447.
- Carmona G, Perera U, Gillett C, Naba A, Law A-L, Sharma VP, Wang J, Wyckoff J, Balsamo M, Mosis F, et al. (2016). Lamellipodin promotes invasive 3D cancer cell migration via regulated interactions with Ena/VASP and SCAR/WAVE. Oncogene 35, 5155–5169.
- Caswell PT, Zech T (2018). Actin-based cell protrusion in a 3D matrix. Trends Cell Biol 28, 823–834.
- Cha J, Ding EA, Carvalho EM, Fowler A, Aghi MK, Kumar S (2024). Collagen VI deposition primes the glioblastoma microenvironment for invasion through mechanostimulation of β -catenin signaling. PNAS Nexus 3, 355.
- Chen J, Ananthanarayanan B, Springer KS, Wolf KJ, Sheyman SM, Tran VD, Kumar S (2020). Suppression of LIM kinase 1 and LIM kinase 2 limits glioblastoma invasion. Cancer Res 80, 69–78.

- Colin A, Kotila T, Guérin C, Orhant-Prioux M, Vianay B, Mogilner A, Lappalainen P, Théry M, Blanchoin L (2023). Recycling of the actin monomer pool limits the lifetime of network turnover. EMBO J 42, e112717.
- Coumans JVF, Davey RJ, Moens PDJ (2018). Cofilin and profilin: Partners in cancer aggressiveness. Biophys Rev 10, 1323-1335.
- Ding Y, Milosavljevic T, Alahari SK (2008). Nischarin inhibits LIM kinase to regulate cofilin phosphorylation and cell invasion. Mol Cell Biol 28, 3742-3756.
- Djuzenova CS, Fiedler V, Memmel S, Katzer A, Hartmann S, Krohne G, Zimmermann H, Scholz CJ, Polat B, Flentje M, et al. (2015). Actin cytoskeleton organization, cell surface modification and invasion rate of 5 glioblastoma cell lines differing in PTEN and p53 status. Exp Cell Res 330, 346-357.
- Doyle AD, Petrie RJ, Kutys ML, Yamada KM (2013). Dimensions in cell migration. Curr Opin Cell Biol 25, 642-649.
- Dull T, Zufferey R, Kelly M, Mandel RJ, Nguyen M, Trono D, Naldini L (1998). A third-generation lentivirus vector with a conditional packaging system. J Virol 72, 8463–8471.
- Ershov D, Phan M-S, Pylvänäinen JW, Rigaud SU, Le Blanc L, Charles-Orszag A, Conway JRW, Laine RF, Roy NH, Bonazzi D, et al. (2022). Track-Mate 7: Integrating state-of-the-art segmentation algorithms into tracking pipelines. Nat Methods 19, 829-832.
- Friedl P, Sahai E, Weiss S, Yamada KM (2012). New dimensions in cell migration. Nat Rev Mol Cell Biol 13, 743-747.
- Garcia JH, Akins EA, Jain S, Wolf KJ, Zhang J, Choudhary N, Lad M, Shukla P, Rios J, Seo K, et al. (2024). Multiomic screening of invasive GBM cells reveals targetable transsulfuration pathway alterations. J Clin Invest 134, e170397.
- Goode, BL, Eskin, J, Shekhar, S (2023). Mechanisms of actin disassembly and turnover. J Cell Biol 222, e202309021.
- Guetta-Terrier C, Monzo P, Zhu J, Long H, Venkatraman L, Zhou Y, Wang P, Chew SY, Mogilner A, Ladoux B, et al. (2015). Protrusive waves guide 3D cell migration along nanofibers. J Cell Biol 211, 683-701.
- Han K, Jeng EE, Hess GT, Morgens DW, Li A, Bassik MC (2017). Synergistic drug combinations for cancer identified in a CRISPR screen for pairwise genetic interactions. Nat Biotechnol 35, 463-474.
- Hilton DM, Aquilar RM, Johnston AB, Goode BL (2018). Species-specific functions of Twinfilin in actin filament depolymerization. J Mol Biol 430, 3323-3336.
- Horita Y, Ohashi K, Mukai M, Inoue M, Mizuno K (2008). Suppression of the invasive capacity of rat ascites hepatoma cells by knockdown of slingshot or LIM Kinasehanh. J Biol Chem 283, 6013-6021.
- Hotulainen P, Paunola E, Vartiainen MK, Lappalainen P (2005). Actindepolymerizing factor and cofilin-1 play overlapping roles in promoting rapid F-actin depolymerization in mammalian nonmuscle cells. Mol Biol Cell 16, 649-664.
- Jacquemet G, Hamidi H, Ivaska J (2015). Filopodia in cell adhesion, 3D migration, and cancer cell invasion. Curr Opin Cell Biol 36, 23-31.
- Kelly MD, Pawlak MR, Zhan KH, Shamsan GA, Gordon WR, Odde DJ (2024). Mutual antagonism between CD44 and integrins in glioblastoma cell traction and migration. APL Bioeng 8, 036102.
- Kim Y, Kumar S (2014). CD44-mediated adhesion to hyaluronic acid contributes to mechanosensing and invasive motility. Mol Cancer Res 12, 1416-1429.
- Klemke M, Kramer E, Konstandin MH, Wabnitz GH, Samstag Y (2010). An MEK-cofilin signalling module controls migration of human T cells in 3D but not 2D environments. EMBO J 29, 2915-2929
- Kobayashi M, Nishita M, Mishima T, Ohashi K, Mizuno K (2006). MAPKAPK-2-mediated LIM-kinase activation is critical for VEGF-induced actin remodeling and cell migration. EMBO J 25, 713-726.
- Kotila T, Wioland H, Enkavi G, Kogan K, Vattulainen I, Jégou A, Romet-Lemonne G, Lappalainen P (2019). Mechanism of synergistic actin filament pointed end depolymerization by cyclase-associated protein and cofilin. Nat Commun 10, 5320.
- Lee S, Kumar S (2020). Cofilin is required for polarization of tension in stress fiber networks during migration. J Cell Sci 133, jcs243873.
- McCollum CO, Didychuk AL, Liu D, Murray-Nerger LA, Cristea IM, Glaunsinger BA (2023). The viral packaging motor potentiates Kaposi's sarcoma-associated herpesvirus gene expression late in infection. PLOS Pathog 19, e1011163.
- McGrath JL, Osborn EA, Tardy YS, Dewey CF, Hartwig JH (2000). Regulation of the actin cycle in vivo by actin filament severing. Proc Natl Acad Sci USA 97, 6532-6537.
- Moffat J, Grueneberg DA, Yang X, Kim SY, Kloepfer AM, Hinkle G, Pigani B, Eisenhaure TM, Luo B, Grenier JK, et al. (2006). A lentiviral RNAi library

- for human and mouse genes applied to an arrayed viral high-content screen. Cell 124, 1283-1298.
- Mohindra P, Zhong JX, Fang Q, Cuylear DL, Huynh C, Qiu H, Gao D, Kharbikar BN, Huang X, Springer ML, et al. (2023). Local decorin delivery via hyaluronic acid microrods improves cardiac performance, ventricular remodeling after myocardial infarction. Npj Regen Med 8, 1-14.
- Monzo P, Chong YK, Guetta-Terrier C, Krishnasamy A, Sathe SR, Yim EKF, Ng WH, Ang BT, Tang C, Ladoux B, et al. (2016). Mechanical confinement triggers glioma linear migration dependent on formin FHOD3. Mol Biol Cell 27, 1246-1261.
- Morgens DW, Wainberg M, Boyle EA, Ursu O, Araya CL, Tsui CK, Haney MS, Hess GT, Han K, Jeng EE, et al. (2017). Genome-scale measurement of off-target activity using Cas9 toxicity in high-throughput screens. Nat Commun 8, 15178.
- Nagai S, Moreno O, Smith CA, Ivanchuk S, Romagnuolo R, Golbourn B, Weeks A, Seol HJ, Rutka JT (2011). Role of the cofilin activity cycle in astrocytoma migration and invasion. Genes Cancer 2, 859-869
- Nishita M, Tomizawa C, Yamamoto M, Horita Y, Ohashi K, Mizuno K (2005). Spatial and temporal regulation of cofilin activity by LIM kinase and Slingshot is critical for directional cell migration. J Cell Biol 171, 349-359.
- Oser M, Yamaguchi H, Mader CC, Bravo-Cordero JJ, Arias M, Chen X, Des-Marais V, van Rheenen J, Koleske AJ, Condeelis J (2009). Cortactin regulates cofilin and N-WASp activities to control the stages of invadopodium assembly and maturation. J Cell Biol 186, 571-587.
- Pathak A, Kumar S (2012). Independent regulation of tumor cell migration by matrix stiffness and confinement. Proc Natl Acad Sci USA 109, 10334-10339.
- Petrie RJ, Yamada KM (2012). At the leading ed of three-dimensional cell migration. J Cell Sci 125, 5917-5926.
- Poincloux R, Collin O, Lizárraga F, Romao M, Debray M, Piel M, Chavrier P (2011). Contractility of the cell rear drives invasion of breast tumor cells in 3D Matrigel. Proc Natl Acad Sci USA 108, 1943-1948.
- Pollard TD, Borisy GG (2003). Cellular motility driven by assembly and disassembly of actin filaments. Cell 112, 453-465.
- Ponta H, Sherman L, Herrlich PA (2003). CD44: From adhesion molecules to signalling regulators. Nat Rev Mol Cell Biol 4, 33-45.
- Ridley AJ, Schwartz MA, Burridge K, Firtel RA, Ginsberg MH, Borisy G, Parsons JT, Horwitz AR (2003). Cell migration: Integrating signals from front to back. Science 302, 1704-1709.
- Sahai E, Olson MF, Marshall CJ (2001). Cross-talk between Ras and Rho signalling pathways in transformation favours proliferation and increased motility. EMBO J 20, 755-766.
- Salz A, Gurniak C, Jönsson F, Witke W (2020). Cofilin1-driven actin dynamics controls migration of thymocytes and is essential for positive selection in the thymus. J Cell Sci 133, jcs238048.
- Sanjana NE, Shalem O, Zhang F (2014). Improved vectors and genome-wide libraries for CRISPR screening. Nat Methods 11, 783-784.
- Sanz-Moreno V, Marshall CJ (2010). The plasticity of cytoskeletal dynamics underlying neoplastic cell migration. Curr Opin Cell Biol 22, 690-696.
- Schindelin J, Arganda-Carreras I, Frise E, Kaynig V, Longair M, Pietzsch T, Preibisch S, Rueden C, Saalfeld S, Schmid B, et al. (2012). Fiji: An open-source platform for biological-image analysis. Nat Methods 9, 676-682.
- Schulze M, Fedorchenko O, Zink TG, Knobbe-Thomsen CB, Kraus S, Schwinn S, Beilhack A, Reifenberger G, Monoranu CM, Sirén A-L, et al. (2016). Chronophin is a glial tumor modifier involved in the regulation of glioblastoma growth and invasiveness. Oncogene 35, 3163-3177.
- Scott RW, Hooper S, Crighton D, Li A, König I, Munro J, Trivier E, Wickman G, Morin P, Croft DR, et al. (2010). LIM kinases are required for invasive path generation by tumor and tumor-associated stromal cells. J Cell Biol 191, 169-185.
- Shibue T, Brooks MW, Weinberg RA (2013). An integrin-linked machinery of cytoskeletal regulation that enables experimental tumor initiation and metastatic colonization. Cancer Cell 24, 481-498.
- Shishkin S, Eremina L, Pashintseva N, Kovalev L, Kovaleva M (2016). Cofilin-1 and other ADF/cofilin superfamily members in human malignant cells. Int J Mol Sci 18, 10.
- Southwick FS (2000). Gelsolin and ADF/cofilin enhance the actin dynamics of motile cells. Proc Natl Acad Sci USA 97, 6936-6938.
- Stone OJ, Pankow N, Liu B, Sharma VP, Eddy RJ, Wang H, Putz AT, Teets FD, Kuhlman B, Condeelis JS, et al. (2019). Optogenetic control of cofilin and α TAT in living cells using Z-lock. Nat Chem Biol 15, 1183–1190.
- Tinevez J-Y, Perry N, Schindelin J, Hoopes GM, Reynolds GD, Laplantine E, Bednarek SY, Shorte SL, Eliceiri KW (2017). TrackMate: An open and extensible platform for single-particle tracking. Methods 115, 80-90.

- Tojkander S, Gateva G, Husain A, Krishnan R, Lappalainen P (2015). Generation of contractile actomyosin bundles depends on mechanosensitive actin filament assembly and disassembly. eLife 4, e06126.
- Toole BP (1990). Hyaluronan and its binding proteins, the hyaladherins. Curr Opin Cell Biol 2, 839–844.
- Tran VD, Kumar S (2021). Transduction of cell and matrix geometric cues by the actin cytoskeleton. Curr Opin Cell Biol 68, 64–71.
- Wang H, Tao L, Jin F, Gu H, Dai X, Ni T, Feng J, Ding Y, Xiao W, Qian Y, et al. (2017). Cofilin 1 induces the epithelial-mesenchymal transition of gastric cancer cells by promoting cytoskeletal rearrangement. Oncotarget 8, 39131–39142.
- Wang W, Eddy R, Condeelis J (2007). The cofilin pathway in breast cancer invasion and metastasis. Nat Rev Cancer 7, 429–440.
- Wang W, Mouneimne G, Sidani M, Wyckoff J, Chen X, Makris A, Goswami S, Bresnick AR, Condeelis JS (2006). The activity status of cofilin is directly related to invasion, intravasation, and metastasis of mammary tumors. J Cell Biol 173, 395–404.
- Wang X, Zou S, Ren T, Zhao L-J, Yu L-F, Li X-Y, Yan X, Zhang L-J (2021). Alantolactone suppresses the metastatic phenotype and induces the apoptosis of glioblastoma cells by targeting LIMK kinase activity and activating the cofilin/G-actin signaling cascade. Int J Mol Med 47, 68.
- Wolf KJ, Lee S, Kumar S (2018). A 3D topographical model of parenchymal infiltration and perivascular invasion in glioblastoma. APL Bioeng 2, 31903–31903.

- Wolf KJ, Shukla P, Springer K, Lee S, Coombes JD, Choy CJ, Kenny SJ, Xu K, Kumar S (2020). A mode of cell adhesion and migration facilitated by CD44-dependent microtentacles. Proc Natl Acad Sci 117, 11432–11443.
- Wyckoff JB, Pinner SE, Gschmeissner S, Condeelis JS, Sahai E (2006). ROCK- and myosin-dependent matrix deformation enables protease-independent tumor-cell invasion in vivo. Curr Biol 16, 1515–1523.
- Yamada KM, Sixt M (2019). Mechanisms of 3D cell migration. Nat Rev Mol Cell Biol 20, 738–752.
- Yamaguchi H, Condeelis J (2007). Regulation of the actin cytoskeleton in cancer cell migration and invasion. Biochim Biophys Acta 1773, 642–652
- Yamaguchi H, Lorenz M, Kempiak S, Sarmiento C, Coniglio S, Symons M, Segall J, Eddy R, Miki H, Takenawa T, et al. (2005). Molecular mechanisms of invadopodium formation. J Cell Biol 168, 441–452.
- Yap CT, Simpson TI, Pratt T, Price DJ, Maciver SK (2005). The motility of glioblastoma tumour cells is modulated by intracellular cofilin expression in a concentration-dependent manner. Cell Motil 60, 153–165.
- Yoshioka K, Foletta V, Bernard O, Itoh K (2003). A role for LIM kinase in cancer invasion. Proc Natl Acad Sci USA 100, 7247–7252.
- Zebda N, Bernard O, Bailly M, Welti S, Lawrence DS, Condeelis JS (2000). Phosphorylation of Adf/cofilin abolishes Egf-induced actin nucleation at the leading edge and subsequent Lamellipod extension. J Cell Biol 151, 1119–1128.